Performance **AN**d **AC**curacy in **E**lectrical Bio**A**ctivity Recordings (**PANACEA**): A High-Performance, Wireless, Multi-instrument for Potentiometric and Amperometric Recording of Biosignals

Georgios C. Zafeiropoulos[a,1], Konstantinos I. Papadimitriou[b,1], Emmanuel M. Drakakis[b,*]

[a] *Department of Bioengineering and Center for Neurotechnology, Imperial College of Science, Technology and Medicine, London SW7 2AZ, UK*
[b] *Department of Bioengineering, Imperial College of Science, Technology and Medicine, London SW7 2AZ, UK*

Abstract

This paper presents the design, testing and quantitative evaluation of a high-performance, low-power, portable multi-instrument ($107x79mm^2$), capable of recording important biosignals accurately and in real-time. This highly versatile system has the ability to transmit the captured bio-data back to the user either in a wired (HDMI cable) or wireless (ZigBee protocol) manner, depending on the targeted application. The biological information that can be recorded by the proposed instrument spans a wide range of bio-potentials and bio-amperometric signals. The proposed instrument is split into two complementary "sub-instruments", where one is operating as the front-end device, responsible for the accurate, low-noise signal detection and transmission, while the second "sub-instrument" is operating as the "base station", responsible for the collection and further processing of the captured data. For wired transmission (e.g to the user's PC) the front end module can operate independently, however, for wireless transmission both "sub-instruments" are required (transmitter-base station architecture). For wireless transmission, each of the two "sub-instruments" is equipped with dedicated 2Mbps ZigBee radio transceivers and both parts are controlled by a small area embedded FPGA module. The front-end device features two distinct sections: (a) a current/voltage to voltage section comprising six potentiometry and two transimpedance amplifier-based amperometry channels. These eight in total analogue channels are converted into digital form by means of a 24bit, voltage input, Analogue-to-Digital Converter (ADC) and (b) a four channel, commercially available switched-capacitor-based ADC Integrated Circuit (IC), which converts input charge to digital data with

*Corresponding author
Email address: e.drakakis@ic.ac.uk (Emmanuel M. Drakakis)
[1] Joint Lead Authorship

16 or 20bit resolution at 3.125kSPS. The paper presents a plethora of measured wired and wireless experimental results, corresponding to most well-known biomedical and other biological/physical signals including: EEG, ECoG, EMG, ECG, PPG, intracardiac atrial fibrillation (AF) signals, cell media/tissue biopotential, drosophila H1-cell spiking signals and pH sensing using commercially available electrodes. The portable/wearable poly-instrument is suitable for Intensive Care Unit (ICU), High Dependancy Unit (HDU) as well as home monitoring.

Keywords: High-performance, Wireless, Biosignal, Potentiometry, Amperometry, EEG, ECoG, ECG, EMG, ZigBee Protocol
2018 MSC: 00-01, 99-00

---

1. INTRODUCTION

One of the most critical everyday healthcare procedures is the collection of physiological/biological signals from patients. Its significance lies in the fact that by observing such biosignals and by their subsequent analysis and vital information extraction using advanced computational tools, clinical conclusions regarding patient health status and therapeutic interventions can be drawn [1]. With regards to biosignals, a plethora of them can be monitored (e.g. brain, cardiac, muscle, chemical, etc.) concurrently or individually.

Consequently, instruments capable of performing high accuracy/precision and real-time biosignal recording are required. It could be argued that these two factors are among the most important ones because there exists the general necessity for the slightest change in the signal codifying a certain condition or physiology to be captured *(high accuracy and precision)*, when it happens *(real-time)*.

In the past several systems have been designed, each of them with different capabilities. Many of them are oversized offering predominantly wired communications. However, nowadays, technology advancement allows for the realisation of wireless portable instruments the size of a business card, or smaller, depending on the application. Several of them have been proposed, commercially available [2] or not [3, 4, 5, 6, 7], albeit with limitations in the number and the variety of their signal acquisition capability. Device portability, measured signal versatility and remote transmission of the monitored physiological signals are parameters, which add significant practical value towards patients' health monitoring: the ability to monitor a patient's multiple biosignals in ambulatory conditions and while performing everyday tasks.

Additionally, the concept of the Internet of things (IoT) has given a boost to the sensor research field, practically making sensors (and sensing) a necessity for everyday applications. Many IoT devices have physical, chemical and/or other sensors attached that can perform measurements with high sensitivity and accuracy [8, 9]. As a result, the realisation of the means for reliable, practical, high-performance, handy and continuous (or not) interfacing and monitoring with them has become essential.

By considering the aforementioned and evaluating the capabilities of the already existing monitoring systems, we present here a low-cost, high-performance recording instrument that can be used in many environments (clinical, ambulatory, home) and can record potentiometry signals (biopotentials, chemical and physical signals) necessary both for acute conditions and general physiological or physical monitoring. The proposed instrument's features (low-cost, wireless, high precision, real-time and portable) could make it a valuable tool in the hands of medical care staff.

The paper is organised as follows: Part 2 presents the instrument itself and its electrical characteristics. Part 3 discusses several signals (biological and physical) that the instrument is capable of recording, together with the methods used for data acquisition. Subsequently, we provide proof-of-concept measured data accompanied by a discussion on recorded instrument's accuracy.

2. INSTRUMENT DESIGN

The instrument constitutes an aggressive miniaturisation and a wireless generalisation of a piece of *wired-only* bioinstrumentation proposed in the past by our group, tailored for traumatic brain injury monitoring [10]. The new instrument comprises of two "sub-instruments": **i)** the front-end device, which is responsible for the accurate, low-noise signal detection and transmission of the data (wireless or wired) and **ii)** the base station, which receives the collected data and is able to further process them. When wired transmission is required (e.g. to the user's PC), the front-end module can stand independently, whereas for the wireless transmission the complementary "base station" is required.

2.1. Front-End Board

The front-end device of the new instrument, see Figs. 1, 2 and Table 1, is divided into two main sections: **i)** the potentio-/amperometry section, designed around the ADS1298 ($\Delta\Sigma$) ADC IC and its capabilities. The ADS1298 IC offers eight (8) low-power, simultaneous sampling, 24-bit resolution recording channels with built-in programmable gain amplifiers (gain range x1 to x12). Out of the 8 channels, the proposed instrument offers six (6) channels for potentiometric (bio)sensors interface and two (2) for amperometric (bio)sensors interface. Each potentiometric channel incorporates a low-offset, high-input impedance operational amplifier (opamp), followed by a constant gain stage of x11, resulting into a total of x132 analogue gain. Amperometry in this section is offered by means of a transimpedance amplifier topology (TIA). The generated currents that can be captured range from few tens of pAs to tens of nAs. The TIA interface comprises high-valued, ultra-high-precision resistors and low-input bias and offset current opamps. Each channel output is in voltage form and is fed into the ADS1298 IC;

Table 1: Electrical Characteristics of the Front-End Board (see Figs. 1 and 2).

	Front-End Board		
	Sections		
Characteristics	**Amperometry (DDC114)**	**TIA Amperometry**	**Potentiometry (ADS1298)**
Number of Input Channels	2	2	6
Resolution (bits)	16/20	—	24
Sampling Rate (kSPS)	3.125	—	0.5 - 32
Input Bias Current (pA)	0.1	0.003	0.2
Total Analog Current Supply (mA)	~ 14	~ 3.9	~ 18.5
Total Digital Current Supply (mA)	~ 0.5	—	~ 0.5
Size (cm)	10.7 x 7.9		
Medically Graded	Yes		
IC Controller	Spartan3e — 48MHz — FPGA		
Wireless Capability	IEEE 802.15.4 based wireless protocol		
Power Supply	6V (4xAA - 2500mAh batteries)		
Battery Powered Operation	Both sections ~ 8h	ADS1298 Only ~ 25h	DDC114 Only ~ 12.5h

ii) the ultra-low amperometry section, which comprises the DDC114 ADC chip, allowing for current recording by means of switched-capacitor topology (SC). The DDC114 ADC, due to its dual-switched integrator design, allows for continuous current monitoring similar to that of TIA-based amperometry, making it suitable for biosensor monitoring but with significantly less noise. Two current inputs are available. The recording current range capability of the DDC114 extends from few hundreds of fAs to uAs. Its output is in digital voltage form. To minimize interferences from surface leakage currents, copper guard rings have been placed around the high-impedance input nodes of the IC; the TIA amperometry input nodes have been guarded similarly. Moreover, a potentiostats section is available, necessary for running most of the electroanalytical experiments. The potentiostats offer adjustable reference voltages: **a)** from +2.5V to -2.5V and **b)** from +5V to -5V. This section is shared between the TIA and SC amperometry.

Last but not least, the instrument supports two ways of communication, either wired or wireless. For the wireless solution, two radio frequency (RF) modules are used for the (wireless) communication of the front-end device with the base station. Two modules have been used, firstly because the device has been designed in such a way that it could operate as a whole or in sections, and secondly, in this way the user is able to set the data rate of the ADC chips at the required level without the necessity to drive them through a single transceiver. This allows for higher temporal resolution potentiometry and amperometry. As a result, the amperometry section using the DDC114 ADC IC is allocated a

dedicated RF module, while the TIA amperometry and potentiometry section (ADS1298 ADC IC), are assigned a second RF module.

The wireless transceivers are Atmel®'s AT86RF213 modules and support communication based on the IEEE 802.15.4 protocol. The advantage of the specific RF over other wireless protocols (i.e. Wi-Fi, Bluetooth) is the combination of the following parameters[11]: **i)** requires the least SNR for best bit error rate (BER) performance, which is important given that several radio services (e.g. GSM900, GSM1800, 2.4GHz ISM, 5.3GHz LAN, TV bands, etc.) are present at a typical hospital environment, a primary location for the proposed instrument use. **ii)** offers radio-link robustness to interference while ensuring top notch performance and low cost, which is feasible through direct-sequence spread-spectrum (DSSS) technique. Advantages of the DSSS technique are numerous, with the most important ones being the larger operating distance, reduced cross-talk interference, inherent security and less static noise [11]. **iii)** the coexistence of the 802.15.4 with the Wi-Fi and Bluetooth in the 2.4GHz ISM has been empirically, analytically and circumstantially studied. The studies have concluded that the 802.15.4 protocol, compared to the other two RF protocols, shows better performance in the face of surprisingly large amounts of interference [12, 13, 14, 15].

In terms of antenna selection, the 2.4GHz $\lambda/4$ wave monopole antenna, 21mm long with nominal gain of 0dBi, omni-directional design and SMA-plug fixing has been chosen, due to important parameters such as its size, cost and performance. Finally, the wired solution has been realised using a mini-HDMI port. The HDMI protocol is not utilised, rather we use the number of *copper* connections (19 wires) an HDMI cable offers. As in the wireless communication solution, half of them are used for the ADS1298 IC section data and half for the DDC114 IC section data.

2.2. Base Station Board

The base station, shown in Figs. 3 and 4, is the complementary part of the front-end (see Table 2 for its electrical characteristics). All the data captured and processed by the front-end side are wirelessly transmitted to the dedicated RF side of the base station and subsequently are driven to the digital-to-analog converters (DAC) for the regeneration of the transmitted signal.

Table 2: Electrical Characteristics of the Base Station Board (see Figs. 3 and 4)

	Base Station Board	
	Sections	
Characteristics	**Amperometry (DDC114)**	**Potentiometry (ADS1298) & TIA Amperometry**
Number of Output Channels	8	16
Resolution (bits)	16	16
Size (cm)	9.7 x 9.7	
Medically Graded	Yes	
IC Controller	Spartan3e — 48MHz —FPGA	
Wireless Capability	IEEE 802.15.4 based wireless protocol	
Power Supply	220V AC, 50Hz	

There are four (4) DACs on the base station board. Two of them are responsible for the wireless communication part and two for the wired solution. The DAC converts digitised data back to analog form, which allows for the interfacing of the base station with visualisation suites, such as PowerLab®. However, one can use the USB2.0 interface that is provided by the FPGA solution to redirect the data from the transceiver to the PC without the need of a DAC. Switching between wired and wireless data transmission has been designed to be automatic. A signal, generated on the base station device, indicates in the software (interrupt logic) the presence of the HDMI connection and the data transmission switches to the wired solution, and vice versa.

Finally, as in the front-end case, the same FPGA solution has been used for the control of the base station and the programming of the ICs (RFs and DACs), see Figs. 3 and 4.

3. Measured Results

Numerous potentiometric and amperometric biosignals have been recorded with the new instrument (Table 3 illustrates a number of the recorded potentiometric biosignals and their characteristics), serving a wide range of applications. In this study, our primary goal is to provide evidence of faithful wireless capability. A way to do that is by comparing a wirelessly and wire transmitted signal from the same (bio)sensor. Our proposed measurement protocol (see Fig. 5) is described below: the analog signal from the same (bio)sensor is fed into the ADC input where it is digitized and then is transmitted wirelessly and wired to the base station. There, it is driven through the corresponding dedicated DAC (wired/wireless) and finally is sampled with the help of PowerLab® (PLAB) to the PC where it is visualised using the PowerLab®'s accompanied software LabChart®.

Table 3: Voltage related biosignals and their characteristics [45, 46]

Signal	**Bandwidth**	**Amplitude**	**Invasiveness**
Spikes	100 - 10kHz	50 - 500μV	Invasive
LFP	0.5 - 200Hz	10μ - 1mV	Invasive
EEG	0.5 - 100Hz	1 - 20μV	Non-invasive
ECoG	0.5 - 200Hz	5 - 100μV	Moderately invasive
EMG	7 - 500Hz	50μ - 2mV	Minimally or non-inasive
ECG	0.05 - 150Hz	0.1 - 5mV	Non-invasive

At this stage a root mean square error (RMSE) and a normalised root mean square error (NRMSE) calculation is performed between the two transmitted signals to assess the instrument's faithful wireless capability and the signals' integrity. The normalisation for the NRMSE calculation is performed over the mean of the reference signal; the wired signal, when wired vs. wireless measurements are compared and the raw signal, when only wired transmissions are taking place, e.g. neuronal spike recordings. The use of PowerLab® is chosen mainly because of its wide acceptance by the medics, which also acts as a measured signal integrity validation. Apart from the aforementioned reasons, the interfacing with an external recording device, such as Powerlab®, proves the proposed instrument's capability to integrate functionally with existing signal recording systems and introduce wireless communications, while maintaining signal integrity. [2]

For the comparison recordings (wired vs. wireless), the minimum distance between the transmitter and the receiver was two (2) meters, due to the length of the HDMI-to-miniHDMI cable, though we have confirmed the reliable radio operation up to 5m. The signals have been recorded within typical electronics lab susceptible to noise.

Table 4: Summary of settings for ADS1298 measurements.

Measurements	**Resolution (bits)**	**Sampling Rate (kSPS)**	**Gain**
EEG, ECG, EMG, PPG	24	1	x132
ECoG, AF, pH, Biopotential, TIA	24	1	x11
Fly H1-cell spikings[3]	16	32	x132

Due to the plethora of measurements performed, the setup of the proposed instrument for each one has been summarized in Table 4. Along with the varying

[2]It has also been verified that the introduction of the DAC operation, which enables the conversion of the recorded signals to analog signals ready to be acquired by PowerLab® has an insignificant effect upon the signal quality.

[3]This setup and the reason why only 16-bits are used in this setup is further explained in Subsection 3.1.8.

parameters in each setup, there are also others that remain constant; those are the amount of data that are actually trasmitted either wired or wirelessly (16bits out of 24bits) and the wireless data rate (2Mbps). The 16bit transmission limitation is due to DAC-PowerLab® use. However, this cannot be seen as a limitation of the proposed wireless data transmission capabilities, because one could use the aforementioned USB2.0 available protocol to collect the data from the base station device with the full 24-bit resolution. Finally, the total amount of data transmitted through the transceiver is the size of a full buffer (640bits), comprising the protocol header(80bits), the actual data(8*16=128bit) and the *dummy* data (432bits). The *dummy* data are a prerequisite of the AT86RF231 to reach the maximum trasmission speed of 2Mbps [16].

Moving to the DDC114 configuration, it is programmed to record a specific range of input current. In our case, the integration time (T_{INT}) is set to 150ms with the integration capacitance (C_{INT}) set equal to 25pF. These settings allow for current measurements of a few fA to a maximum value of 664pA, which is calculated based on (1) and (2) [17]:

$$T_{INT} = \frac{Q_{IN}}{I_{IN_{(max)}}} \tag{1}$$

$$C_{INT} = \frac{Q_{IN}}{V_{REF} - 0.1V} \tag{2}$$

where Q_{IN} = input charge in coulombs, $I_{IN_{(max)}}$ = input in amperes and $V_{REF} = 4.1V$ in our case.

Another parameter that has to be defined, which importantly affects both configurations, is the latency between the wireless and the wired data arrival at the PC. The data captured from the same sensor are transmitted simultaneously both wired and wirelessly. The total wired transmission time adds up to 68μs, while for the wireless case 720μs. This gives a (wireless vs. wired) latency of about 652μs (see Fig. 6 for more details), which is constant for all the wired vs. wireless measurements.

To sum up, some of the recorded signals have been filtered using the available PowerLab® filters. The type and range of each signal's filtering will be specified at the corresponding subsection of the paper. The post-processing (filtering) of the data using the FPGAs is an alternative available solution not used here to preserve our measurement protocol.

3.1. Potentiometric Signals

3.1.1. Electroencephalography (EEG)

EEG is one of the most widely used techniques for monitoring brain activity. Scalp surface electrodes are deployed using the 10-20 gold standard system for electrode placement [18]. It is predominantly used for patient's mental condition assessment [19] but also for other abnormalities in the brain activity, such as epileptic seizures [20].

To assess the instrument's capability to record EEG signals three trials were undertaken. The first was to record the activity from the frontal area of the

brain while there was eye blinking. This method includes movements of the forehead muscles and it is not widely acceptable as an EEG recording capability indicator. The setup for this method were three electrodes in total, with their location being at [21]: **1.** F_{p2} - *Recording Electrode*, **2.** F_{pz} - *Earth Electrode* and **3.** A_2 - *Reference Electrode*. Fig. 7 shows the result from the blinking activity using the aforementioned electrode positioning. RMSE and NRMSE between wired and wirelessly acquired signals for Fig. 7 are equal to $0.0014V$ and 0.23% respectively.

The second trial, Fig. 8, was to capture blinking, however this time from the occipital lobe. This is a more adequate approach. For this test, four electrodes were positioned as follows: **1.** F_3 - *Ground Electrode*, **2.** F_4 - *Reference Electrode*, **3.** O_1 - *Recording Electrode* and **4.** O_2 - *Recording Electrode*.

Finally, the last trial was to record alpha wave (8-12Hz) activity, which is referred to as the most prominent proof of an instrument's capability to measure EEG signals. The setup of the electrodes is the same as the one followed in the second trial. Fig. 9 illustrates band-pass filtered (0.1-60Hz) recordings of EEG alpha wave signals both wired and wireless, from the occipital lobe area as have been annotated by an expert (electrophysiologist). The process follows the pattern of closed eyes (relaxation mode), which induces alpha wave activity, followed by opening the *'oculus uterque'*, which is suppressing the alpha activity.

3.1.2. ElectroCorticography (ECoG)

ECoG is an alternative way to measure electrical activity from the brain. The main difference from the EEG is that the recording takes place from the brain surface (invasive)[22], either using a strip electrode [23] placed on the exposed surface of the brain or a depth electrode [24].

ECoG is widely used in traumatic brain injury (TBI) as well as in brain-machine interfaces (BMI) [25]. In TBI, spreading depolarization (SD) waves are being monitored, which are neuronal and astrocytic depolarizations that propagate across the cerebral cortex [26, 27]. To test the instrument, surrogate,"played back" ECoG signals were used as input to the new instrument. The raw anonymised ECoG signals were originally recorded by means of AD-Tech® strip electrodes and approved wired instruments in the intensive care unit (ICU) complying with appropriate ethical approvals [10].

The ECoG input signal was set to have a period of 10s (or frequency of 0.01Hz) and an amplitude of 20mV, which are approximately the characteristics of a real SD wave produced by a human injured brain. In Fig. 10, both the input and output signals from the recording instrument can be seen. The RMSE and NRMSE between the wired and wireless outputs have been calculated to be equal to $0.0007V$ and 0.2% respectively.

3.1.3. Electromyography (EMG)

EMG is a technique that records the electrical activity of the skeletal muscles. It is used widely to identify traumas at muscle tissue, nerves or in neuromuscular junctions [28, 29, 30]. Generally speaking, two types of electrodes can be used in EMG, either minimally invasive or skin surface ones. For this study, four

skin surface disposable solid gel electrodes (contact size 15x20mm) produced by Unimed®, have been deployed and they have been placed at the following lower side of the upper limp positions:

1. Musculus Extensor Carpi Radialis Longus - *Recording Electrode*
2. Musculus Flexor Carpi Radialis - *Recording Electrode*
3. Elbow bone (Ulna) - *Reference Electrode*
4. Ankle - *Earth Electrode*

Two arm movements have been utilised for the recordings: grasp and tremor. The electrodes' potitioning has been chosen based on [31]. The signal has been band-pass filtered (10-400Hz) [32]. In Fig. 11, the acquired EMG signals using the new instrument are shown, with RMSE and NRMSE values for each electrode to be: Electrode 1 = $0.0256V$ and 2.85% and Electrode 2 = $0.0141V$ and 2.65%. Fig. 12 shows a zoomed-in version of the Electrode-1 traces, the same ones as in Fig. 11. The purpose of this is to illustrate the detailed signal acquisition using either the wired or wireless capabilities of the proposed instrument.

3.1.4. Electrocardiogram (ECG)

ECG is a crucial diagnostic modality, which examines changes in cardiac electrical activity, e.g. rhythm disturbances [33, 34]. ECG uses skin surface electrodes, which detect the electrical current spread throughout the body, caused by the cardiac activity. The unipolar ECG chest leads positioning has been chosen for the testing of the proposed system. More information on the electrodes placement (and the ECG in general) can be found in [35]. The electrodes used for the signal acquisition are the Max-TAB resting electrodes (contact size 20x24mm), produced by Unimed®. Fig. 13 illustrates band-pass filtered (1-150Hz) wired vs. wireless unipolar ECG recordings. The RMSE and NRMSE values are respectively equal to: for LA (Left Arm) $0.0177V$ and 0.22% , LL (Left Leg) $0.0207V$ and 0.16% and RA (Right Arm) $0.0106V$ and 0.27%.

As previously performed in the EMG section (Fig. 12), in order to stress how indistinguishable the two traces (wired and wireless) are from each other, a single QRS complex is plotted (Fig. 14 **(left)**) along with a small, zoomed-in section of the same signal (Fig. 14 **(right)**). Observe the small delay ($\sim 1ms$) characterising the wireless transmission with respect to the wired collection of the same data.

3.1.5. Photoplethysmogram (PPG) measurement

An alternative method to ECG in measuring heart activity is the photoplethysmography (PPG). The method is widely known as pulse oximetry (PO), where the PPG signal by means of an algorithm is translated into a number of heart beats per second. The specific experimental set up consists of two instruments that have been developed within our Lab, the proposed here instrument and the pulse oximetry front-end reported in [36].

The instrument described in [36] uses red (R) and infra-red (IR) light to measure the oxygen in the blood. Its outputs (nA level current within the range of 0.5-3.5Hz) are fed into the custom-made pulse-oximetry prototype IC [36] where they are translated into voltage. The outputs of our customised pulse-oximetry IC were input to the proposed here instrument, where they are digitised and transmitted wirelessly. Results from the aforementioned set up are illustrated in Figure 15.

3.1.6. Multipolar Catheter Measurement - Intracardiac Signal

Atrial Fibrillation (AF) is a cardiovascular disease, which has been characterised as the most common arrhythmia, as well as a primary cause of stroke. One of the ways to treat AF is by observing the ectopic beats of the pulmonary veins (PVs), which have been initiated using high frequency stimulation (HFS), and then apply cauterization of the atrial tissue in the PV junction using an ablation catheter [37, 38].

To monitor PV beats, a multipolar catheter is utilised and inserted into the coronary sinus, which is finally guided into the left atrium (LA) where the recording takes place. More information on AF can be found in [37] and [38]. Surrogate, "played back" data obtained from a 19-pole catheter with mV amplitude and sampled at 2034.5Hz, which become our input test signals.

Figure 16 illustrates the raw input signal and the outputs from the proposed here instrument. There is insignificant difference between the wired and wireless outputs; RMSE and NRMSE have been calculated equal to $0.0076V$ and 0.38% respectively.

3.1.7. Biopotential Measurement

The bioelectrical potential measurement serves as a method for discrimination between healthy and non-healthy (cancerous) omental tissue [39]. Tissue samples are collected through surgery and they are tested *ex vivo*. The experimental setup for medical-based measurements (as described in [39]) consists of: **1.** a tungsten working electrode, **2.** a silver-silver chloride (Ag/AgCl) double junction reference electrode, **3.** an instrumentation amplifier (which is provided by the proposed instrument), **4.** RPMI 1640 cell culture medium (Life Technologies, Carlsbad, CA), **5.** one millilitre (ml) pipette tips and **6.** a beaker. The setup is shown in Figure 17.A.

As in [39], we test the new instrument by means of RPMI-1640 media measurements.The media contains adequate background ions; recording the developed biopotential allows for the establishment of a reference voltage level for tissue voltage measurements. The working tungsten electrode (WE) is touching the media and measures the (dc in practice) potential that is created on the foci, while the reference electrode provides a stable voltage for comparison with the WE. Figure 17.B illustrates wired vs. wireless biopotential measurements. The two traces coincide.

3.1.8. Drosophila Fly H1-cell spikes recording

In order to test the capability of our instrument in full, we recorded neural spike data originating from drosophila fly H1 cells. The data were played back and fed into the instrument's input by means of the Agilent 33220A waveform generator. The data provided were sampled at 20kHz and they had a duration of 8 seconds.

The data that was used for the measurement had a duration of 2.5sec and were played back in an infinite loop. The sample frequency of the ADC of our instrument was set at 32kHz (see Table 1), which is the maximum sample frequency the ADS1298 can support with only 16bit resolution per channel. The current sampling frequency setting has been chosen following the signal's characteristics and more specifically its bandwidth (see Table 3). The results of the measurement can be seen in Figure 18.

The RMSE and NRMSE errors between the raw ("played back") data and the data recorded in a wired manner are equal to $0.118V$ and 0.46% respectively. The successful recording of such spiking data confirms the ability of our instrument to record with high temporal resolution. The wireless transmission of such spiking data with similar temporal resolution is not possible due to the finite (2Mbps) bit rate of the radio. When we record with 32kSPS, we have (for 8 Channels) $16 * 8 = 128 bits/sample$. This means that the total number of bits we need to transmit per second for all 8 channels is $(32000 * 128) = 4.096 Mbits$ (data only - header and dummy data not included), which is more than double the available data rate of the radio.

3.1.9. pH measurements

The current potentiometric measurement aims at confirming the suitability of the proposed instrument for interfacing with commercial sensors. pH measurement was chosen due to its biomedical relevance [40]. The measured pH levels are of: (i) tap water; (ii) distilled water at 16MO.cm, purified by the Purite SELECT Fusion water purification system; (iii) Artificial cerebrospinal fluid (ACSF), with concentrations of $2.7mMKCl$, $147mMNaCl$, $1.2mMCaCl_2$ and $0.85mMMgCl_2$.

Table 5: Summary of the pH measurements taken with the proposed instrument and the commercial sensor. The pH7,pH4 and pH10 solutions were used for the calibration of the sensor (Table 5a). The remaining solutions (Table 5b) are two types of water and ACFS, where their pH level has been measured in terms of the sensor's voltage output and the pH level has been calculated taking into consideration the sensor's calibration curve (Table 5a). The voltage values have been acquired at steady state condition.

(a) Calibration Data

Solution	**Amplitude (V)**
pH-7	-0.147
pH-4	1.831
pH-10	-2.101

(b) Measured pH Data

Solution	**Amplitude (V)**	**pH**
Tap Water	-0.477	7.8
ACSF	-1.28	7.6
Distilled Water	0.855	5.7

The pH sensor used for the measurements is the Atlas Scientific's pH Probe

with a range of up to pH 14. The isopotential point of the sensor is located at pH 7 with 0V output. For every 1 pH level of change the output voltage varies by ±59mV, which depends on the acidic(-) or alkaline(+) character of the solution in question. Prior to measurement, the sensor was calibrated with the solutions provided. Calibration and test measured results are summarised in Table 5.

3.2. Amperometry

3.2.1. T.I.A & Switched-Capacitor-based (DDC114) (see Table 1) measurements

Both amperometric sections serve for low level current measurements. Examples of relevant physiological current signals are the rapid sampling microdialysis-based amperometric measurements of *glucose* and *lactate* levels of the injured human brain tissue [41, 42].

To examine the high-perfomance amperometric recording capabilities of the instrument, both for T.I.A and the DDC114 chip, a Keithley 6221-current generator has been used. A generated current was supplied, ranging between 0 to 100pAs. Figure 19 shows the acquired results. The range for the TIA section was calculated using the 5GΩ nominal value resistor, which enables the read-out of current levels as low as a few tenths of picoamperes. The DDC114 was programmed to measure in the same current levels.

3.2.2. Ultra-low current measurement using the DDC114 and a Photodiode's dark current

In order to examine the proposed instrument's capability to detect and record ultra-low currents, the HAMAMATSU S1087 Si Photodiode was utilised. A photodiode senses light intensity and converts it into current at its output. In our case, the photodiode was used for the measurement of its "dark current", which can be viewed as a naturally encountered ultra low value current source. The setup can be seen in Fig. 20. The photodiode was covered (no incident light upon it) and reversed-biased by means of voltage pulses of appropriate level. The resulting ultra-low current difference pulses were recorded as illustrated in Fig. 21. The DDC114 converts directly charge to voltage exploiting switched-capacitor techniques [17].

In the case of Fig. 21.A, the two reverse applied voltage levels were set to 3 and 5V, while in Fig. 21.B, they were set to 3 and 10V. In accordance with the Hamamatsu S1087 photodiode datasheet [43], the difference between the levels 1 and 2 in Fig. 21.A, corresponds to $400fA$. In Fig. 21.B the difference between levels 3 and 4 corresponds to $1.2pA$.

4. Discussion

4.1. Limitations and Future Improvements

The first set of collected test signals were related to potentiomentry. Successfully measured signals included EEG, ECoG, EMG, ECG, PPG, intra-cardiac signals (AF), biopotential, drosophila H1-cell spikes and finally pH. The next

set of measurements is related to amperometry. More specifically, we demonstrated the successful high-performance acquisition and radio transmission of two types of current data measurement using either customary resistor-based I-to-V amperometry or switched-capacitance based amperometry.

All the aforementioned measurements have been carried out using both the available wired and wireless communications, verifying the proposed instrument's high accuracy and low noise performance. Regarding the recorded signals' quality standard, our clinical experts (see Acknowledgements section), were asked to perform an inspection of the recorded signals and assess their quality. They have concluded that the recorded signals are of quality comparable to their clinical standards and can be used for clinical decision making. Another significant factor that has to be emphasised at this point, is the wireless connectivity and its reliability. No wireless connection "drop-off" was ever observed, even when the proposed instrument was operating in excess of 24h (instrument operated through a power supply).

Despite the good performance, there is room for further improvement. However, limitations on data recording accuracy and performance are not discussed since these are determined by the choice of the specific converter chips. We rather focus our discussion on ways formed for increasing the capabilities of the instrument.

The potentiometry section is currently set to perform only unipolar measurements. This means that the 6-channels of the ADS1298 chip, can only use a single common reference. This can be either the GND/earth of the board or an appropriate biosignal (e.g. right leg recording position) that acts as a reference. The ADS1298 chip allows for bipolar measurements; only minute modifications in the design of the amplification stage would need to take place.

Such change of the input stage design would also call for tuning of the gain control. In this version of Panacea, we have opted for a constant gain stage of x11. This has been introduced bearing in mind that input signals with small amplitudes (μV level) would first need to be amplified enough so as not to rest within the input voltage noise level of the ADS1298. The component ADS1299 could be used for improved noise performance albeit at the expense of generally lower sampling rate. The incorporation of the gain stage and ADS1298 limits the variety of input signals that could be recorded with the instrument. The ADC is able to measure voltage signals in the range of $\pm$ 2.5V. As a result, the highest amplitude input signal, including the x11 constant gain, is $\sim$230mV. Instead of having a constant gain, the inclusion of a Programmable Gain Amplifier (PGA) would allow for an input signal range from μV to V.

A further improvement relates to the use of more than one ADS1298 chips so as to increase the number of channels that are able to interface with a variety of physical and chemical (bio)sensors and record the corresponding data. This way more channels for EEG, ECG, EMG and ECoG would become available.

Discussing higher level but significant improvements, the design of a graphical user interface (GUI) is required [44]. Through this the end-user, by either a touch-screen or a conventional keyboard-mouse configuration will be able to control the instrument. Furthermore and as an extension of the GUI, a database

where the data can be stored (protected and available only to approved user) should be implemented, which also allows for data availability instantly through the Internet to any device with access to it (e.g. smartphones, tablets, etc.).

5. Conclusion

In this paper, a novel bioinstrument has been presented, its various capabilities have been tested and discussed and finally its performance has been assessed quantitatively. It has been shown that the instrument is able to record a plethora of biological and physical signals using both wired and wireless data transmission, which makes it a useful and practical tool to be utilised in a wide range of applications, scenarios and environments.

It is important to stress again that the instrument's front-end is battery operated, with minute power consumption. The on-battery operation duration varies based on the applications in use (see Table. 1). This is because it can provide operation by individual sections and/or as a whole. The potentiometry and amperometry sections of the instrument have shown to provide precise and low-noise measurements. Moreover, its ability to interface with already commercial sensors has been examined and proven.

Aknowledgements

The authors would like to thank Mr Konstantinos Petkos for helping with the debugging of the instrument and participating in the experiments and Dr Ilias Pagkalos for sharing his knowledge in the measurement of the photodiode's dark current. Moreover, Professor Martyn Boutelle's group for sharing information and resources regarding the pH measurements and specifically miss Sharon Jewell for providing her expertise in the field of electrophysiology. We also thank Professor Antony Strong, Dr Nick Linton and Professor Holger Krapp for kindly providing us with raw ECoG/SD ("*artificial*"), Multipolar Catheter and Drosophila Fly H1-cells spiking signals accordingly. Finally, this work was supported by the UK Engineering and Physical Sciences Research Council (EPSRC) [grant number EP/L016737/1] for the Imperial College London Centre for Doctoral Training, the Centre for Neurotechnology.

References

[1] E. S. Berner (Ed.), Clinical Decision Support Systems, Health Informatics, Springer International Publishing, Cham, 2016. URL: http://link.springer.com/10.1007/978-3-319-31913-1. doi:10.1007/978-3-319-31913-1.

[2] Guger Technologies, g.Nautilus by g.tec Medical Engineering, 2016. URL: http://www.gtec.at/Products/Hardware-and-Accessories/g.Nautilus-PRO-Specs-Featureshttp://www.gtec.at/.

[3] L. H. Wang, T. Y. Chen, K. H. Lin, Q. Fang, S. Y. Lee, Implementation of a wireless ECG acquisition SoC for IEEE 802.15.4 (ZigBee) applications, IEEE Journal of Biomedical and Health Informatics 19 (2015) 247–255.

[4] U. Imtiaz, L. Bartolomeo, Z. Lin, S. Sessa, H. Ishii, K. Saito, M. Zecca, A. Takanishi, Design of a wireless miniature low cost EMG sensor using gold plated dry electrodes for biomechanics research, in: 2013 IEEE International Conference on Mechatronics and Automation, IEEE ICMA 2013, 2013, pp. 957–962. doi:10.1109/ICMA.2013.6618044.

[5] L. Boquete, J. M. R. Ascariz, J. Cantos, R. Barea, J. M. Miguel, S. Ortega, N. Peixoto, A portable wireless biometric multi-channel system, Measurement: Journal of the International Measurement Confederation 45 (2012) 1587–1598.

[6] M. Sawan, M. T. Salam, J. Le Lan, A. Kassab, S. Gelinas, P. Vannasing, F. Lesage, M. Lassonde, D. K. Nguyen, Wireless recording systems: From noninvasive EEG-NIRS to invasive EEG devices, IEEE Transactions on Biomedical Circuits and Systems 7 (2013) 186–195.

[7] L. Brown, J. Van De Molengraft, R. F. Yazicioglu, T. Torfs, J. Penders, C. Van Hoof, A low-power, wireless, 8-channel EEG monitoring headset, in: 2010 Annual International Conference of the IEEE Engineering in Medicine and Biology Society, EMBC'10, 2010, pp. 4197–4200. doi:10.1109/IEMBS.2010.5627393.

[8] S. Patel, H. Park, P. Bonato, L. Chan, M. Rodgers, A review of wearable sensors and systems with application in rehabilitation, Journal of Neuro-Engineering and Rehabilitation 9 (2012) 21.

[9] L. Atzori, A. Iera, G. Morabito, The Internet of Things: A survey, Computer Networks 54 (2010) 2787–2805.

[10] K. I. Papadimitriou, C. Wang, M. L. Rogers, S. A. N. Gowers, C. L. Leong, M. G. Boutelle, E. M. Drakakis, High-Performance Bioinstrumentation for Real-Time Neuroelectrochemical Traumatic Brain Injury Monitoring, Frontiers in Human Neuroscience 10 (2016) 1–15.

[11] NXP Laboratories UK, Co-existence of IEEE 802.15.4 at 2.4GHz, Application Note, 2013. Rev. 1, [Accessed 17/10/2017].

[12] ZigBee Alliance, Zigbee and Wireless Radio Frequency Coexistence, White Paper, 2007. Rev. 1, [Accessed 17/10/2017].

[13] A. Sikora, V. Groza, Coexistence of IEEE802.15.4 with other Systems in the 2.4 GHz-ISM-Band, in: 2005 IEEE Instrumentationand Measurement Technology Conference Proceedings, volume 3, IEEE, 2005, pp. 1786–1791. URL: http://ieeexplore.ieee.org/document/1604479/. doi:10.1109/IMTC.2005.1604479.

[14] S. Y. Shin, S. Choi, H. S. Park, W. H. Kwon, Lecture Notes in Computer Science:Packet Error Rate Analysis of IEEE 802.15.4 Under IEEE 802.11b Interference, Springer Berlin Heidelberg, Berlin, Heidelberg, 2005, pp. 279–288. URL: https://doi.org/10.1007/11424505{_}27. doi:10.1007/11424505_27.

[15] S. Y. Shin, J. S. Kang, H. S. Park, Packet error rate analysis of ZigBee under interferences of multiple bluetooth piconets, IEEE Vehicular Technology Conference 6 (2009) 2825–2830.

[16] Atmel Corporation, Low Power 2.4GHz Transceiver for ZigBee, IEEE 802.15.4,6LoWPAN, RF4CE, SP100, WirelessHART and ISM Applications, AT86RF231, Datasheet, 2009. Rev. 1, [Accessed 27/10/2017].

[17] Texas Instruments, Quad Current Input, 20-Bit Analog-To-Digital Converter, DDC114, 2009. Datasheet Rev. 2, [Accessed 17/10/2017].

[18] R. Oostenveld, P. Praamstra, The five percent electrode system for high-resolution EEG and ERP measurements, Clinical Neurophysiology 112 (2001) 713–719.

[19] R. Zhang, M. D. Brandt, W. Schrempf, C. Beste, A.-K. Stock, Neurophysiological mechanisms of circadian cognitive control in RLS patients - an EEG source localization study, NeuroImage: Clinical 15 (2017) 644–652.

[20] O. Faust, U. R. Acharya, H. Adeli, A. Adeli, Wavelet-based EEG processing for computer-aided seizure detection and epilepsy diagnosis, Seizure 26 (2015) 56–64.

[21] J. Tanaka, M. Kimura, N. Hosaka, H. Sawaji, K. Sakakura, K. Magatani, Development of the EEG measurement technique under exercising, in: 2005 IEEE Engineering in Medicine and Biology 27th Annual Conference, IEEE, 2005, pp. 5971–5974. URL: http://ieeexplore.ieee.org/document/1615851/. doi:10.1109/IEMBS.2005.1615851.

[22] E. Asano, C. Juhasz, A. Shah, O. Muzik, D. C. Chugani, J. Shah, S. Sood, H. T. Chugani, Origin and Propagation of Epileptic Spasms Delineated on Electrocorticography, Epilepsia 46 (2005) 1086–1097.

[23] A. J. Strong, M. Fabricius, M. G. Boutelle, S. J. Hibbins, S. E. Hopwood, R. Jones, M. C. Parkin, M. Lauritzen, Spreading and Synchronous Depressions of Cortical Activity in Acutely Injured Human Brain, Stroke 33 (2002) 2738–2743.

[24] T. Jeffcote, J. M. Hinzman, S. L. Jewell, R. M. Learney, C. Pahl, C. Tolias, D. C. Walsh, S. Hocker, A. Zakrzewska, M. E. Fabricius, A. J. Strong, J. A. Hartings, M. G. Boutelle, Detection of Spreading Depolarization with Intraparenchymal Electrodes in the Injured Human Brain, Neurocritical Care 20 (2014) 21–31.

[25] K. Hu, F. Bounni, Z. Williams, Editorial. Advancement in brainmachine interfaces for patients with tetraplegia: neurosurgical perspective, Neurosurgical Focus 43 (2017) E5.

[26] A. Leão, Spreading Depression of Activity in the Cerebral Cortex, Journal of Neurophysiology 7 (1944) 359–390.

[27] J. A. Hartings, M. R. Bullock, D. O. Okonkwo, L. S. Murray, G. D. Murray, M. Fabricius, A. I. Maas, J. Woitzik, O. Sakowitz, B. Mathern, B. Roozenbeek, H. Lingsma, J. P. Dreier, A. M. Puccio, L. A. Shutter, C. Pahl, A. J. Strong, Spreading depolarisations and outcome after traumatic brain injury: a prospective observational study, The Lancet Neurology 10 (2011) 1058–1064.

[28] A. A. Leis, M. P. Schenk, Atlas of Nerve Conduction Studies and Electromyography, Oxford University Press, 2012. URL: `http://www.oxfordmedicine.com/view/10.1093/med/9780199754632.001.0001/med-9780199754632`. doi:`10.1093/med/9780199754632.001.0001`.

[29] A. Balbinot, A. S. Júnior, G. W. Favieiro, Decoding Arm Movements by Myoelectric Signal and Artificial Neural Networks, Intelligent Control and Automation 04 (2013) 87–93.

[30] H. J. Chong, S. J. Kim, E. K. Lee, G. E. Yoo, Analysis of surface EMG activation in hand percussion playing depending on the grasping type and the tempo, Journal of Exercise Rehabilitation 11 (2015) 228–235.

[31] Y. Nakaya, C. Ishii, T. Nakakuki, Y. Nishitani, M. Hikita, Distinction of Abnormality of Surgical Operation on the Basis of Surface EMG Signals, IEEJ Transactions on Industry Applications 132 (2012) 241–249.

[32] E. A. Clancy, E. L. Morin, R. Merletti, Sampling, noise-reduction and amplitude estimation issues in surface electromyography, Journal of Electromyography and Kinesiology 12 (2002) 1–16.

[33] M. Eyuboglu, Y. Karabag, S. Karakoyun, O. Senarslan, Z. Tanriverdi, B. Akdeniz, Usefulness of fragmented QRS in hypertensive patients in the absence of left ventricular hypertrophy, The Journal of Clinical Hypertension (2017) 1–5.

[34] K. T. Nguyen, E. Vittinghoff, T. A. Dewland, J. W. Dukes, E. Z. Soliman, P. K. Stein, J. S. Gottdiener, A. Alonso, L. Y. Chen, B. M. Psaty, S. R. Heckbert, G. M. Marcus, Ectopy on a Single 12Lead ECG, Incident Cardiac Myopathy, and Death in the Community, Journal of the American Heart Association 6 (2017) e006028.

[35] R. E. Klabunde, Cardiovascular Physiology Concepts, Lippincott Williams & Wilkins (2012) 256.

[36] K. N. Glaros, E. M. Drakakis, A Sub-mW fully-integrated pulse oximeter front-end, IEEE Transactions on Biomedical Circuits and Systems 7 (2013) 363–375.

[37] P. B. Lim, L. C. Malcome-Lawes, T. Stuber, I. Wright, D. P. Francis, D. W. Davies, N. S. Peters, P. Kanagaratnam, Intrinsic Cardiac Autonomic Stimulation Induces Pulmonary Vein Ectopy and Triggers Atrial Fibrillation in Humans, Journal of Cardiovascular Electrophysiology 22 (2011) 638–646.

[38] P. Ganesan, E. M. Cherry, A. M. Pertsov, B. Ghoraani, Characterization of Electrograms from Multipolar Diagnostic Catheters during Atrial Fibrillation, BioMed Research International 2015 (2015).

[39] W. Wu, K. Vitharana, T. Gorgy, A. Paterson, P. Cunnea, H. Gabra, C. Fotopoulou, M. G. Boutelle, E. M. Drakakis, A method for voltage measurements of cancerous vs non-cancerous omentum, Proceedings of the Annual International Conference of the IEEE Engineering in Medicine and Biology Society, EMBS 2015-Novem (2015) 7514–7517.

[40] R. Ilyas, K. Chow, J. G. Young, What Is the Best Method to Evaluate Urine pH? A Trial of Three Urinary pH Measurement Methods in a Stone Clinic, Journal of Endourology 29 (2015) 70–74.

[41] M. L. Rogers, D. Feuerstein, C. L. Leong, M. Takagaki, X. Niu, R. Graf, M. G. Boutelle, Continuous online microdialysis using microfluidic sensors: Dynamic neurometabolic changes during spreading depolarization, ACS Chemical Neuroscience 4 (2013) 799–807.

[42] M. L. Rogers, C. L. Leong, S. A. Gowers, I. C. Samper, S. L. Jewell, A. Khan, L. McCarthy, C. Pahl, C. M. Tolias, D. C. Walsh, A. J. Strong, M. G. Boutelle, Simultaneous monitoring of potassium, glucose and lactate during spreading depolarization in the injured human brain Proof of principle of a novel real-time neurochemical analysis system, continuous online microdialysis, Journal of Cerebral Blood Flow & Metabolism 37 (2017) 1883–1895.

[43] Hamamatsu Photonics, Si photodiodes, Ceramic package photodiodes with low dark curent, S1087, 2014. Datasheet Rev. 1, [Accessed 17/10/2017].

[44] X. Yue, E. M. Drakakis, M. Lim, A. Radomska, H. Ye, A. Mantalaris, N. Panoskaltsis, A. Cass, A real-time multi-channel monitoring system for stem cell culture process, IEEE Transactions on Biomedical Circuits and Systems 2 (2008) 66–77.

[45] J. Holleman, F. Zhang, B. Otis, Ultra Low- Power Integrated Circuit Design for Wireless Neural Interfaces, Springer New York, NEW YORK, 2011. URL: `https://link.springer.com/book/10.1007{%}2F978-1-4419-6727-5`.

[46] T. Denison, K. Consoer, W. Santa, A.-T. Avestruz, J. Cooley, A. Kelly, A 2 μW 100 nV/rtHz Chopper-Stabilized Instrumentation Amplifier for Chronic Measurement of Neural Field Potentials, IEEE Journal of Solid-State Circuits 42 (2007) 2934–2945.

[47] I. Pagkalos, M. L. Rogers, M. G. Boutelle, E. M. Drakakis, A High-Performance Application Specific Integrated Circuit for Electrical and Neurochemical Traumatic Brain Injury Monitoring, ChemPhysChem (2018) 1–12.

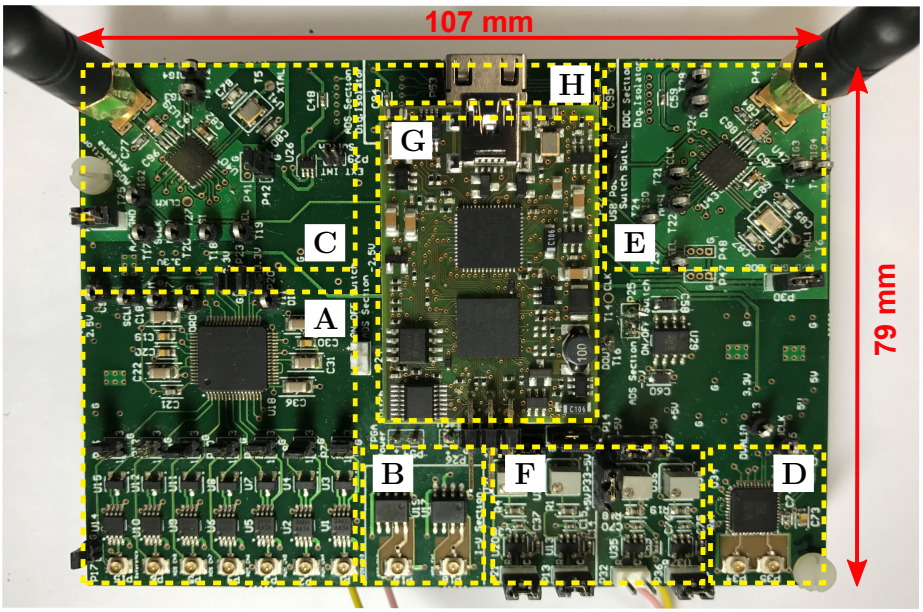


Figure 1: Front-End Board. The fabricated twin-radio electronic instrument. **(A, B, C)** Potentiometry and transimpedance amperometry sections with a dedicated transceiver (TX). **(D, E)** Switch-capacitor amperometry section with a dedicated transceiver (TX). **(F)** Potentiostats section. **(G)** A small area embedded field-programmable gate array (FPGA) module, which acts as a controller but also provides USB communications. **(H)** Wired communications section with the base station.

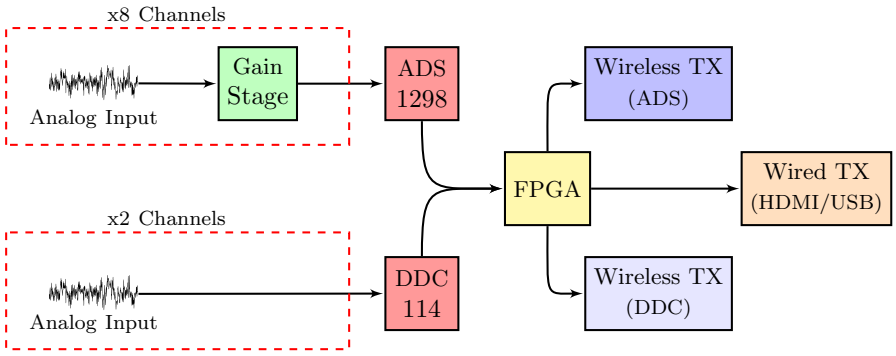


Figure 2: Basic operational architecture of the Panacea Front-end (see Fig. 1). Six (6) potentiometry and four (4) amperometry analog signals are driven through the ADCs (ADS1298, DDC114) to an FPGA. Finally, the captured data are transmitted wired and/or wirelessly to the Base station (see Fig. 3) or a PC. Each ADC has its own, dedicated wireless transceiver.

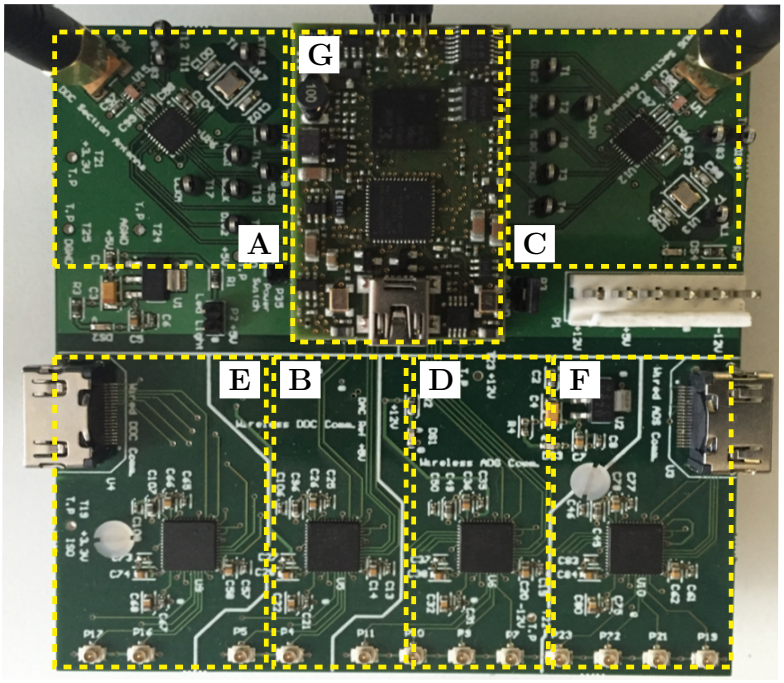


Figure 3: Base station Board. The fabricated instrument. **(A,B)** Potentiometry and TIA amperometry tranceiver (RX) section with its dedicated DAC. **(C,D)** SC amperometry tranceiver (RX) section with its dedicated DAC. **(E,F)** Dedicated DAC sections for wired communications with the Front-end. **(G)** A small area embedded field-programmable gate array (FPGA) module, which acts as a controller but also provides USB communications.

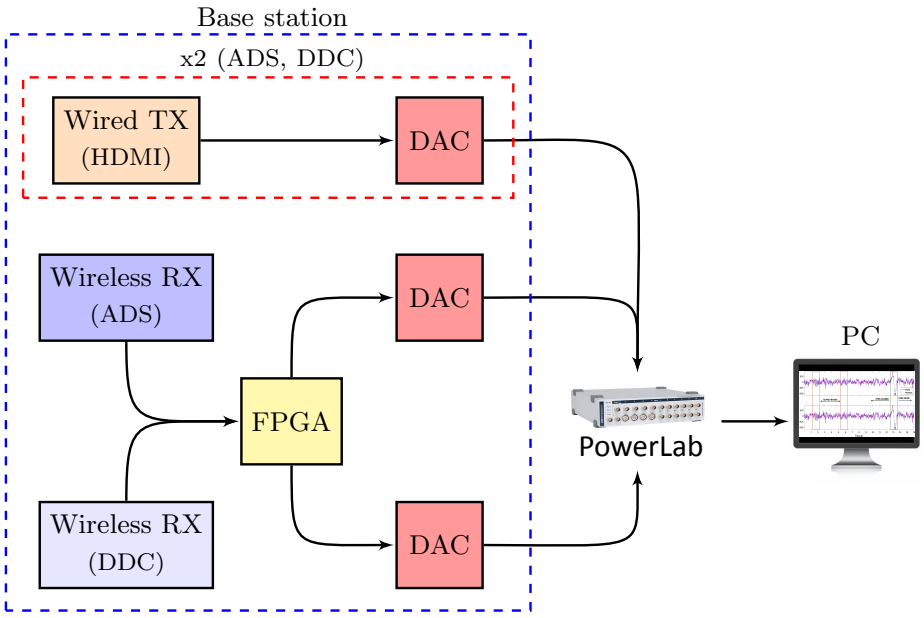


Figure 4: Basic operational architecture of the Panacea Base station (see Fig. 3). The wired and/or wireless transmitted data from the Front-end, are captured by the Base station. Then, through the DACs, are driven to PowerLab® and finally to a PC. Each wired and wireless communication path has its own dedicated DAC.

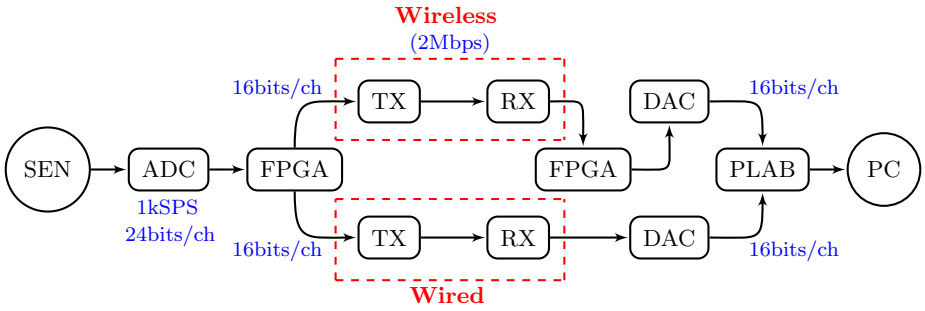


Figure 5: Measurements protocol data flow diagram, where the two distinct data routes (wireless and wired transmission) are illustrated.

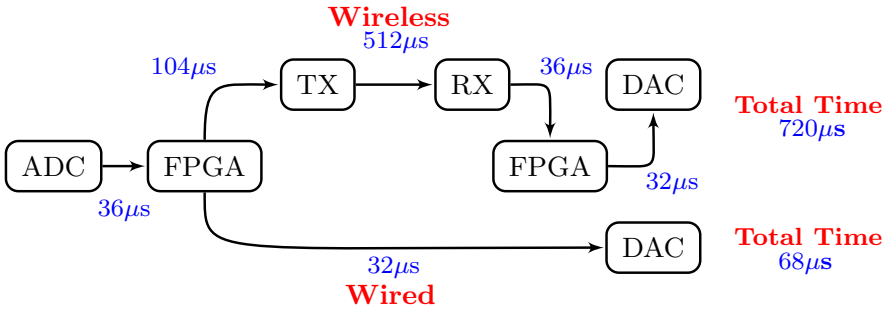


Figure 6: Latency between the wired and wireless transmission. The time difference is $\sim$ 652μs. This is constant for all the measurements that include both transmissions.

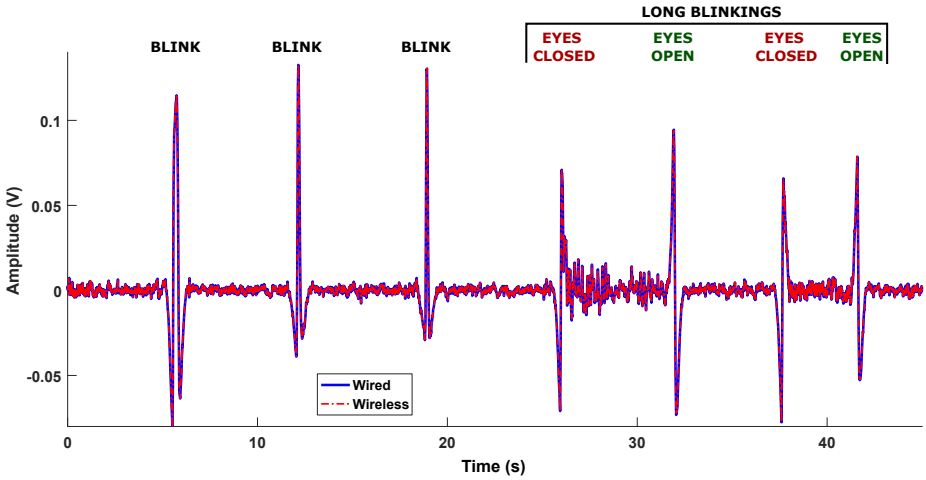


Figure 7: Wired vs. wireless recording of two different blink types. The first three are instantaneous blinks of the eyes, while the following two are longer blinkings (Wired vs. Wireless RMSE and NRMSE = $0.0014V$ and 0.23% respectively).

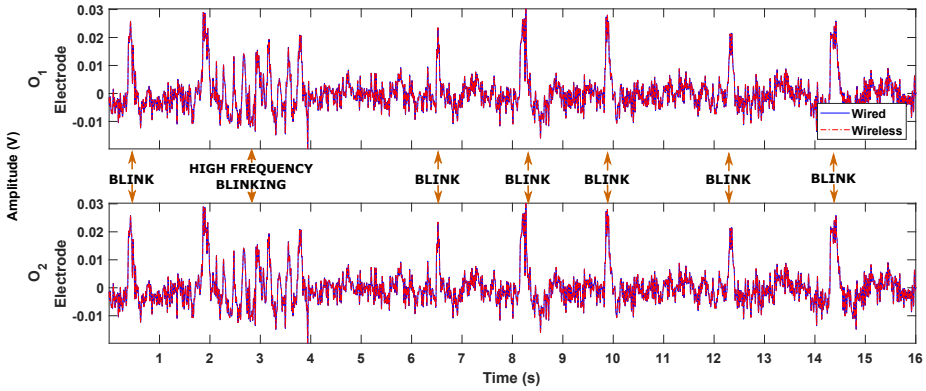


Figure 8: Wired vs. wireless recording of two different blink types. Single blink of the eyes or high frequency blinking. Both traces (wired and wireless) coincide in both electrodes.

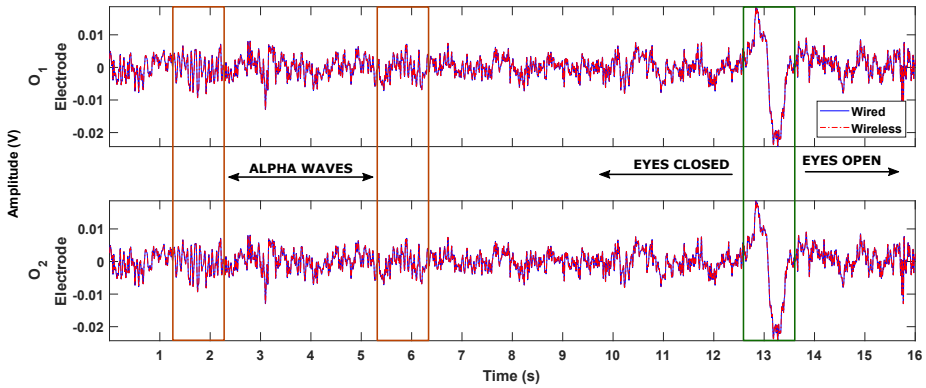


Figure 9: Demonstration of alpha wave activity recordings, as annotated by an expert, from O_1 and O_2 electrode position. The traces have been simultaneously recorded using the proposed instrument's wired and wireless capability. Both traces (wired and wireless) coincide in both electrodes.

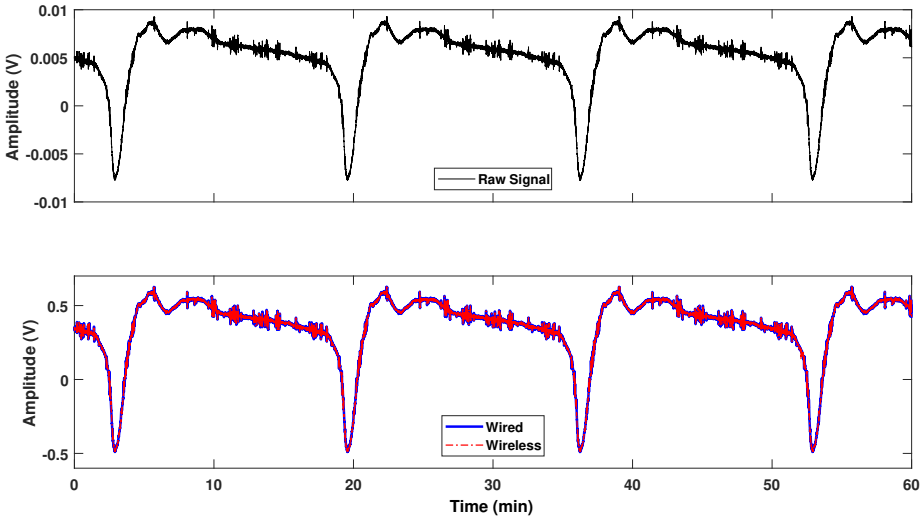


Figure 10: The top trace (black) is the raw input ECoG signal. The bottom two traces are the wired and wireless outputs as they have been recorded by the instrument. All the signals have been visualised simultaneously using PowerLab®. (wired vs. wireless RMSE and NRMSE = $0.0007V$ and 0.2% respectively).

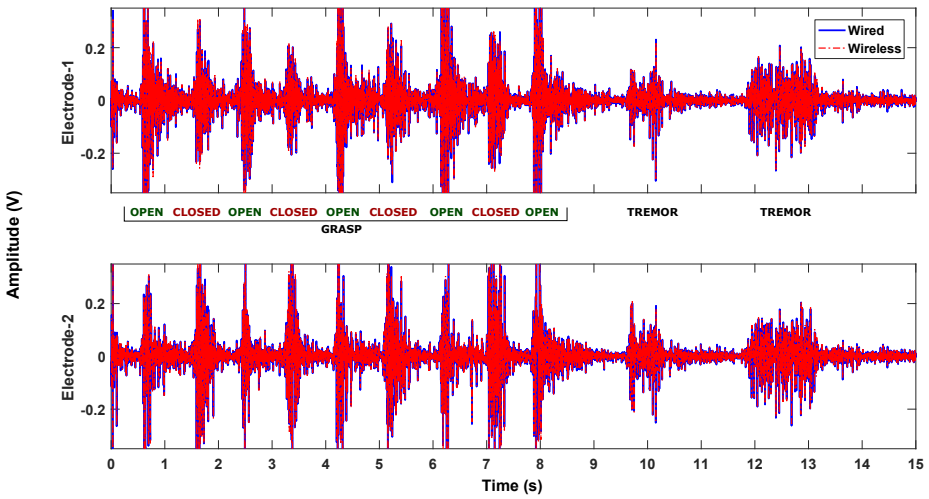


Figure 11: Top traces (wired and wireless outputs) have been recorded by the new instrument from the same electrode. Same for the bottom traces. Two arm movements are simulated: "Grasp" and "Tremor". All the signals have been recorded simultaneously. (wired vs. wireless RMSE and NRMSE for Electrode 1 = $0.0256V$ and 2.85% and Electrode 2 = $0.0141V$ and 2.65% respectively).

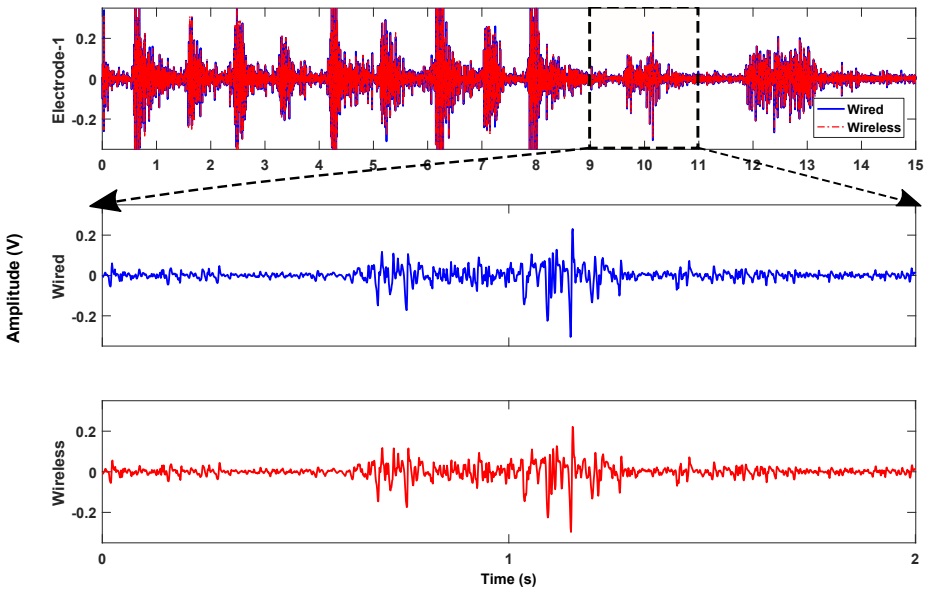


Figure 12: Wired vs. wireless EMG recordings from Electrode-1. Zoomed-in version facilitates the visual comparison between wirelessly recorded and wired data.

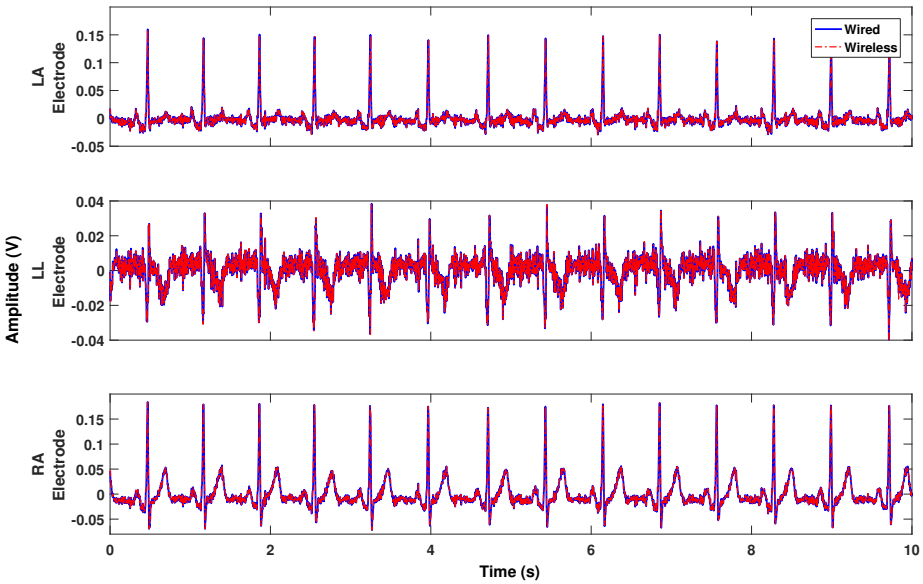


Figure 13: Wired vs. wireless ECG measurements using unipolar set up. Each electrode (LA,LL,RA) was using as a reference an electrode placed on the right leg ankle. (wired vs. wireless RSME and NRMSE: LA = $0.0177V$ and 0.22%, LL = $0.0207V$ and 0.16%, RA = $0.0106V$ and 0.27%).

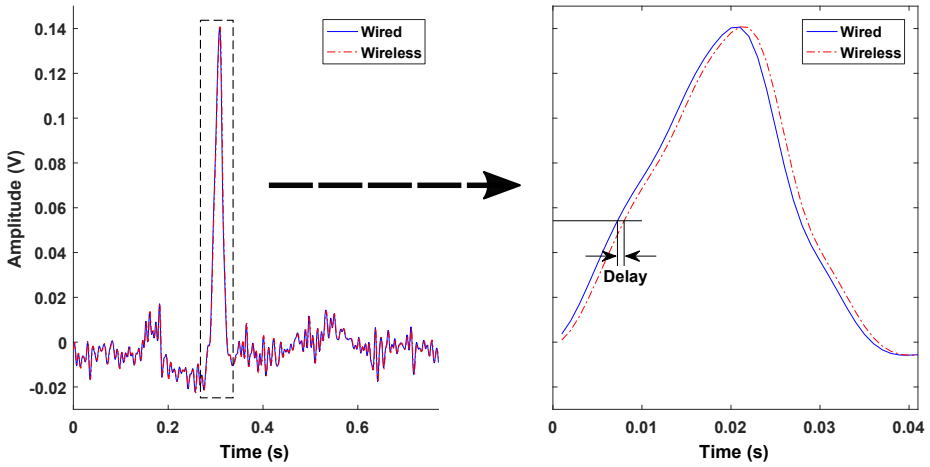


Figure 14: Comparison between wired and wireless communications. **(Left)** Plot of the same QRS complex from both the wireless and wired outputs of the instrument. **(Right)** Delay between the wireless and the wired data due to transeiver operation. The delay is $\sim 1ms$.

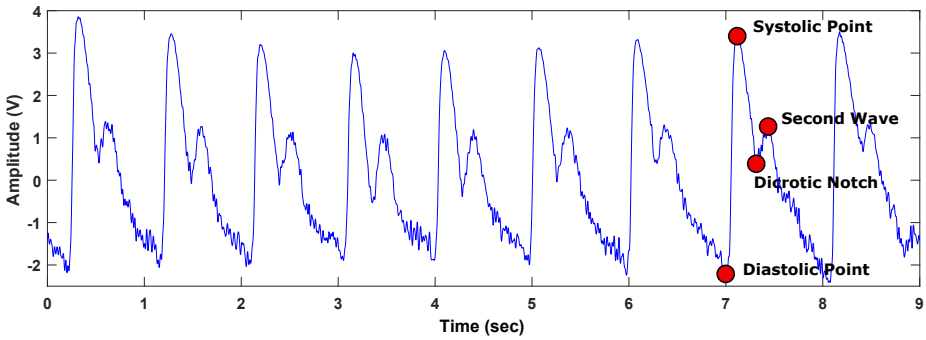


Figure 15: PPG test signal recorded wirelessly by the proposed instrument. The specific signal is the signal read by the red (R) emitting sensor. The two typical PPG peaks can be observed. The diastolic point and the systolic point is the difference in light between the most and least oxygenated blood condition. In case there is dicrotic notch, a second wave is following.

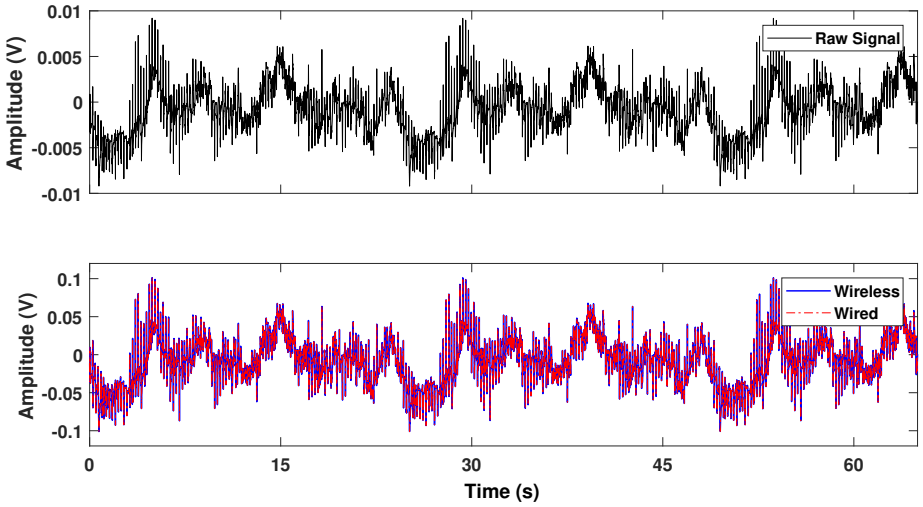


Figure 16: Multipolar Catheter data recordings. (**TOP**) Raw "played back" signal from the Agilent 33220A waveform generator, which becomes the input signal to the proposed instrument. (**BOTTOM**) Wired and wireless recorded data. (wired vs. wireless RMSE and NRMSE = $0.0076V$ and 0.38% respectively).

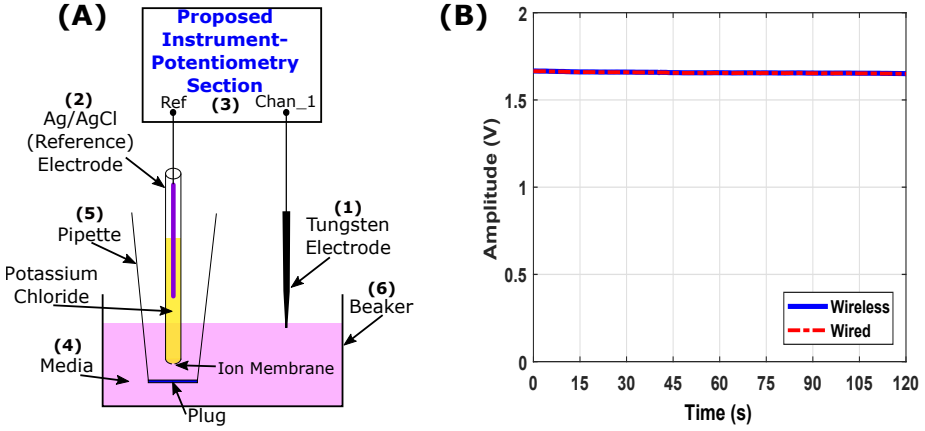


Figure 17: **(A)** Setup for biopotential (media/tissue) measurements [39]. **(B)** wired vs. wireless biopotential. The two traces(wired and wireless) coincide.

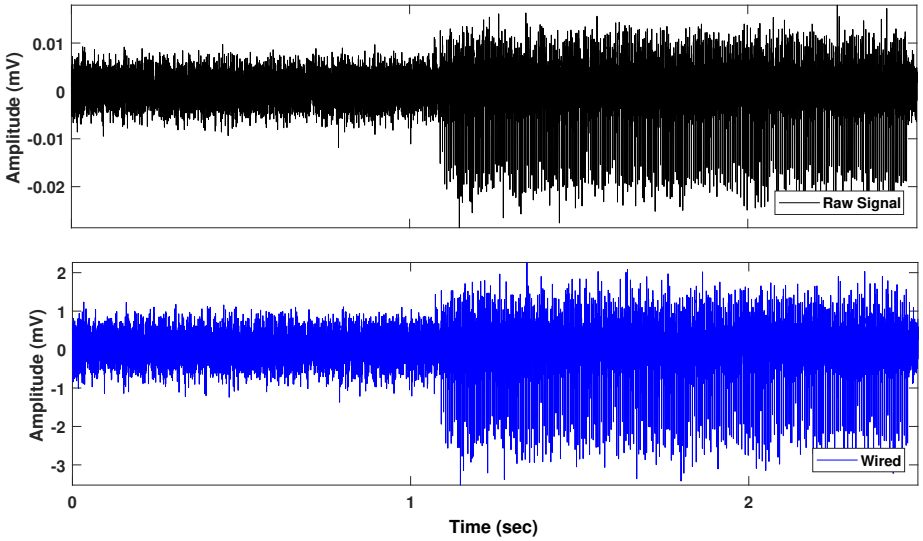


Figure 18: Drosophila fly H1-cell spike recording using the proposed instrument. **(TOP)** The raw data as fed from the waveform generator. **(BOTTOM)** The data as recorded using the proposed instrument. (raw vs. wired RMSE and NRMSE = $0.118V$ and 0.46% respectively).

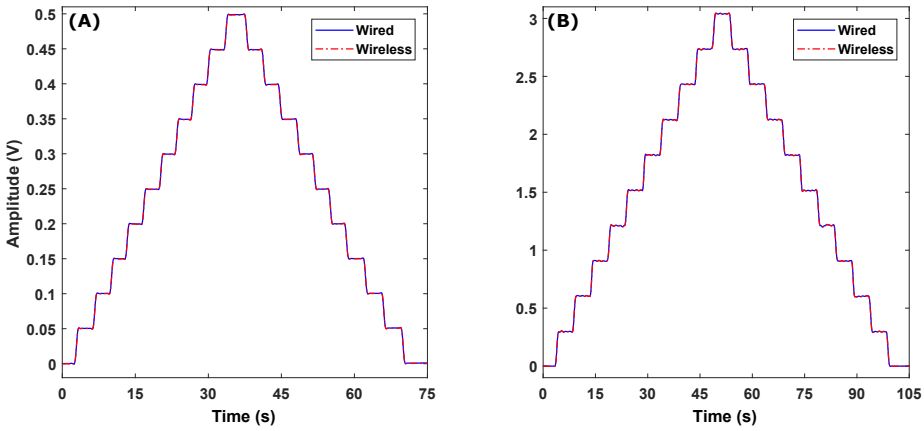


Figure 19: Wired vs. wireless amperometry using both technologies available. The input current for both is generated by the Keithley 6221. The input current is presented in steps of 10pA and ranges from 0 to 100pA. **(A)** I-V measurements using the transimpedance (G = 5GΩ) amplifier setup (NRMSE $< 0.12\%$). **(B)** DDC114 measurements (NRMSE $< 0.09\%$).

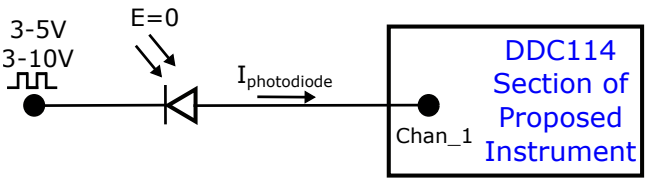


Figure 20: Dark current measurement setup, similar to one reported in [47]. Reverse-biasing voltage pulses are applied to the photodiode while its current output is connected to the input of our DDC114-based front-end. The recorded output voltage pulses by our instrument correspond to ultra-low value dark current pulses [43] shown in Fig. 21.

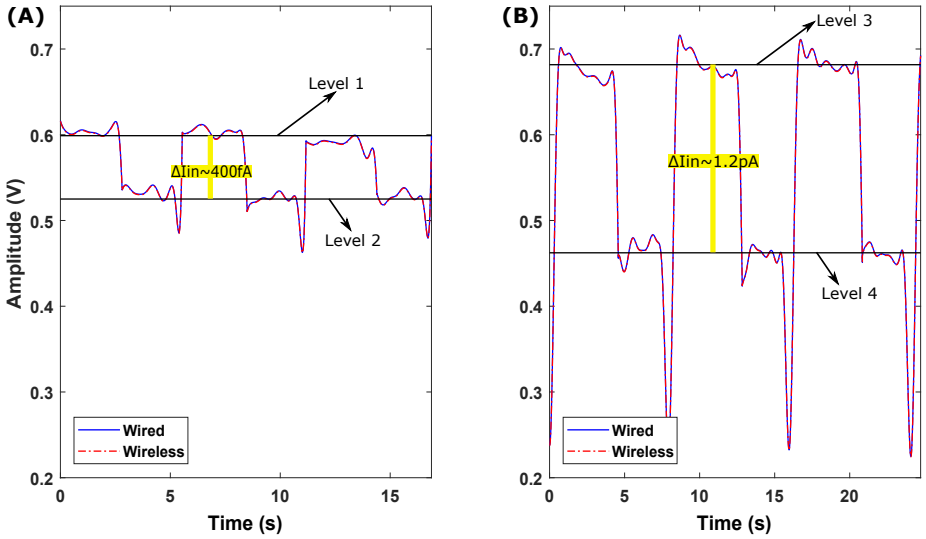


Figure 21: Wired vs. wireless DDC114 measurements exploiting the dark current of a reversed-biased photodiode as an ultra-low value current source. **(A)** The difference between the two levels of voltage (levels 1 and 2) correspond to a difference of $400fA$. **(B)** The difference between the two levels of voltage (levels 3 and 4) correspond to a difference of $1.2pA$ [43]. The wired and wireless data coincide.